Publishing Excellence
Inspiring Progress
ARISTON PUBLICATIONS
ChemSci Advances
ISSN: 2997-9587 www.aristonpubs.com/chemsci-advances https://doi.org/10.69626/csa.2024.0014

RESEARCH ARTICLE

# Ni-Doped $LaFeO_3$ Microspheres Composed of Nanoparticles for the Photocatalytic Degradation of Organic Dye

**Sameena R. Mulani [1*], Santosh Bimli [1], Rajendra Bunkar [1], Manopriya Samatham[1], Ekta Choudhary[1,2], Ajay Patil [1], Suman Yadav [1], Ankit Yadav [1], Harshada Jadhav [1], Aayushi Miglani[2]**

**ABSTRACT:** Ni-doped $LaFeO_3$ (LFO) microsphere consisting of nanoparticles are synthesized by the hydrothermal route and used for the degradation of Rhodamine B (RhB) organic dye. The structural, morphological, and optical analysis is confirmed by the various characterization techniques, i.e., X-ray diffraction (XRD), field emission scanning electron microscopy (FESEM), and UV-Visible spectroscopy. The all Ni-doped LFO catalyst shows excellent efficiency towards the photocatalytic degradation of RhB dye. LFNO-0.2 catalyst shows the highest degradation efficiency of 89.44% with rate constant (k) and correlation coefficient ($R^2$) of 0.013304 $min^{-1}$ and 0.989, respectively. The radical scavenging suggests the active involvement of $O_2^-$ and $h^+$ participates in the efficient degradation. Moreover, the material possesses excellent cyclic stability for the continuous Xenon lamp exposure of 540 min. Overall, the Ni-doped LFO can serve as one of the finest materials for wastewater remediation by means of photocatalytic dye degradation.

**Keywords:** $LaFeO_3$; Ni doping; Rhodamine B; Scavenger; Photocatalysis

**Received: 14 January 2024; Revised: 23 February 2024; Accepted: 07 March 2024; Published Online: 20 March 2024**

## 1. INTRODUCTION

The world is facing energy crises and health issues, and worldwide, the most critical problem is associated with the lack of clean and fresh water. Water contamination is one of the most critical issues across the globe, especially in rural areas of India. Industrial and agricultural effluents, radioactive waste, and domestic effluents are key factors that contribute to water pollution. Several industries, namely leather tanning, food processing, paper and paint, textile industry, and hair colorings, discharge the synthetic dyes directly into water streams, which is the foremost hazard for human beings and the ecosystem [1, 2]. Direct contact with the colored waste can severely damage the human tissue, skin, and pulmonary systems and have carcinogenic and mutagenic effects. Additionally, they produce adverse effects on aquatic life by limiting their photosynthetic activity as it interfere with light penetration [3].

A wide range of treatments, such as oxidation of water, nano-filtration, reverse osmosis, ion-exchange membranes, and biological methods, have been investigated over the last two decades for photocatalytic water purification. Further, these techniques are expensive and suffer from secondary waste formation and biodegradability [4]. Nevertheless, cost-effective photo-catalytic processes can reduce the level of water contaminants to meet environmental regulations as it totally rely on the use of solar energy and overcome the limitations of the above-cited treatments as it deliver the advantages like mild reaction conditions, eco-friendly, no waste disposal problem, and complete mineralization [5].

$TiO_2$ was one of the first utilized metal oxide semiconductors for efficient dye degradation owing to properties like low cost, non-toxic nature, and abundant

[1] Department of Metallurgical Engineering and Materials Science, Indian Institute of Technology Indore, Simrol, Indore, 453552 India.
[2] Department of Physics, Indian Institute of Technology Indore, Simrol, Indore, 453552 India.

*Author to whom correspondence should be addressed:
phd1801205002@iiti.ac.in (Sameena Mulani)

availability. However, it suffers from the disadvantage of a wide bandgap utilizing only UV light and not harvesting the visible light [6]. ZnO was another photocatalysis explored after $TiO_2$, but it also suffers from the photo-corrosion effect [7]. Furthermore, various single metal oxide semiconductors, like $WO_3$ [8], $SnO_2$ [9], $CeO_2$ [10], NiO [11], and $ZrO_2$ [12], etc. utilized for the degradation of organic dye molecules, are yet to overcome the low quantum efficiency, short carrier diffusion length, low conductivity, wide band gap and reduces photocatalytic efficiency. To overcome the downfalls mentioned above, novel binary metal oxide photocatalysts with the chemical formula $A_xB_yO_z$ (where A and B are La, Mn, Fe, Mg, Ca, Ti, Co, Ni, V, etc) are being developed [13]. These include the $ABO_3$ perovskite with the variable oxidation state of 2+, 3+, and 4+, etc., found to deliver band gap in the visible range, chemical and structural stability, and resistance to photo corrosion, which are the desirable qualities for the efficient degradation of dye molecules.

Among all perovskite compounds, $LaFeO_3$ (LFO) is selected as a catalyst because it possesses a conduction band potential of 0.025 eV, non-toxicity, and a small bandgap of 2.07 eV, and it possesses high conductivity at intermediate (400-600°C) temperature [14]. The LFO possesses high electronic conductivity and availability of $O_2^-$ ions under visible light radiation [15]. Further, Ni-doped LFO perovskites are gaining attention owing to their remarkable physicochemical characteristics. The high structural stability and excellent optoelectronic properties result in enhanced photocatalytic activity [16]. The doping of $Ni^{2+}$ into the LFO matrix causes a distorted structure, which arises because of the difference between the ionic radii of $Ni^{2+}$ and $Fe^3$. The lattice mismatch results in reduction in activation energy and improves the conductivity [17]. As activation energy decreases, the rate of reaction increases, and this process speeds up the rate of reaction by reducing activation energy; hence, it helps in increasing the rate of photocatalytic reaction. Ni doping at the Fe site in LFO is reported to improve thermal expansion near yttria-stabilized zirconia (YSZ), oxygen permeability, and electrical conductivity, which enhances the rate of acetyl acetate combustion [18]. Similarly, Ni doping also provides higher photocatalytic [19] and desalination activity [20]. Herein, Ni-doped LFO microspheres are synthesized by the cost-effective hydrothermal method, characterized by various characterization techniques and utilized for the photocatalytic degradation of rhodamine B (RhB) dye.

## 2. EXPERIMENTAL DETAILS

Ferric nitrate (Fe $(NO_3)_3$. $9H_2O$), Lanthanum nitrate ($La(NO_3)_3$. $6H_2O$), Nickel nitrate (Ni $(NO_3)_2$. $6H_2O$), and Citric acid ($C_6H_8O_7$) were purchased from SRL Chem. All chemicals were analytic grade and used without further purification. LFO and 20% Ni-doped LFO (LFNO-0.2) were synthesized using a hydrothermal technique. Required stoichiometric amounts of analytic grade metal precursors and citric acid were mixed in 15 ml distilled water and stirred for 30 min at room temperature. The homogeneously mixed solution was transferred to teflon-lined stainless steel autoclave. The autoclave was kept for 12 h at 180 ºC for the formation of the LFO microsphere. The collected powder was washed with DI water and ethanol to remove the surfactant and dried at 100 ºC overnight. Afterward, the dried powder was annealed at 800 ºC for 6h for phase formation and used for further characterization.

## 3. RESULTS AND DISCUSSION

The morphological characteristics of LFO and LFNO were investigated employing a Field Emission Scanning Electron Microscope (FESEM). Fig. 1 shows the formation of LFO and LFNO microspheres encompassing nanoparticles of diameter 120-140 nm. Interestingly, the microsphere diameter has been reduced to 1.5-2 µm after doping 20 % of Ni. Moreover, the diameter of nanoparticles present in those microspheres has also reduced to 30-40 and 10-20 nm, respectively. The interconnection of nanoparticles has resulted in the formation of mesoporous microsphere. The reduced particle size might provide a larger surface area and is expected to provide more active sites for the adsorption and desorption of dye molecules, which improve the dye degradation activities. Moreover, Ni doping induces defect levels in the parent compounds, which prevents the electron-hole pair recombination rate.

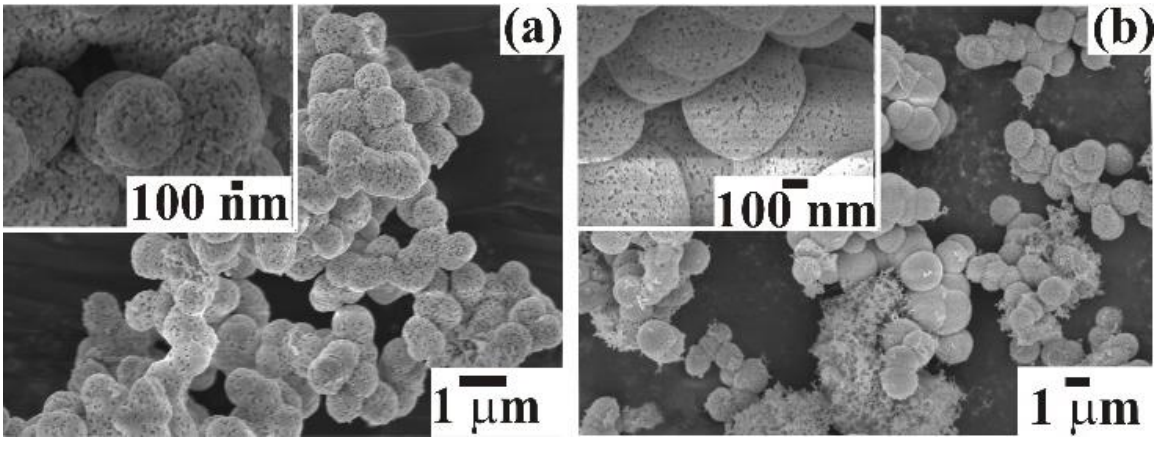


**Fig. 1.** FESEM micrograph of (a) pristine and (b) Ni-doped $LaFeO_3$ microspheres.

 

XRD pattern was used to confirm the phase purity and crystalline nature of pristine and Ni-doped samples. Fig. 2 shows XRD spectra of LFO and LFNO-0.2. The characteristics XRD peaks observed at 2θ of 22.9, 32.3, 39.8, 46.3, 52.17, 57.7, 67.4, and 76.7º corresponding to the (101), (121), (220), (202), (141), (240), (242), and (204) planes, respectively, of orthorhombic crystal in the space group of Pnma (JCPDS: 37-1493) and lattice parameters a = 5.565Aº, b = 7.839Aº, and c = 5.577Aº. All observed diffraction peaks correspond to the orthorhombic perovskite structure observed in pristine LFO. Impurity peaks confirm the minor presence of the orthorhombic $La_2O_3$ phase. The entry of $Ni^{2+}$ ions into the LFO lattice has resulted in a minor variation in the positions of the peaks than that of LFO and is assigned to the larger grain growth [21].

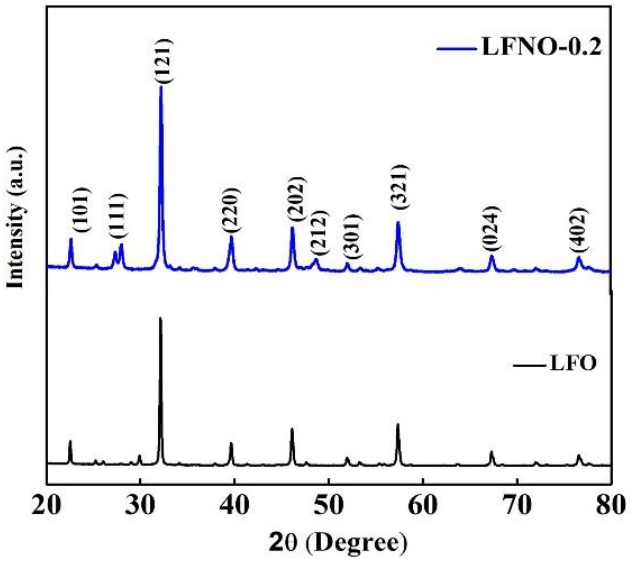


**Fig. 2.** XRD pattern of LFO and LFNO-0.2 samples.

The optical properties of LFO and LFNO-0.2 were evaluated using UV-Visible absorbance spectroscopy. Fig. 3 depicts the absorbance spectra of both samples, indicating good absorption in the whole spectrum from 200-800 nm. This wide absorption provides good activity toward photocatalytic dye removal.

The photocatalytic degradation activity was evaluated using 30 mg catalyst dose. Fig. 4 (a-b) shows the UV-Visible spectra collected for the LFO and LFNO-0.2 catalyst for 30 ppm RhB dye solution. RhB shows a strong absorption peak at 554 nm and decreases gradually as exposure time increases to 180 min for all three samples [22]. The absence of any extra peaks during irradiation terminates the possibility of forming LFO and/or dye derivatives. The degradation performance was evaluated by considering the maximum absorption peak at 554 nm. During photocatalytic measurements, we observed the diminished color after 180 min of visible light radiation, indicating the structure of RhB dye starts de-ethylated with the destruction of its conjugated structure.

Fig. 4(c) depicts the histogram of the degradation performance of RhB with time. The initial concentration ($C_o$) and concentration at reaction time t (Ct) of the RhB dye solution were monitored to estimate the photocatalytic dye removal rates using Eq. (1).

$$Dye\ degradation\ (\%) = \frac{C_t - C_0}{C_0} \times 100 \quad (1)$$

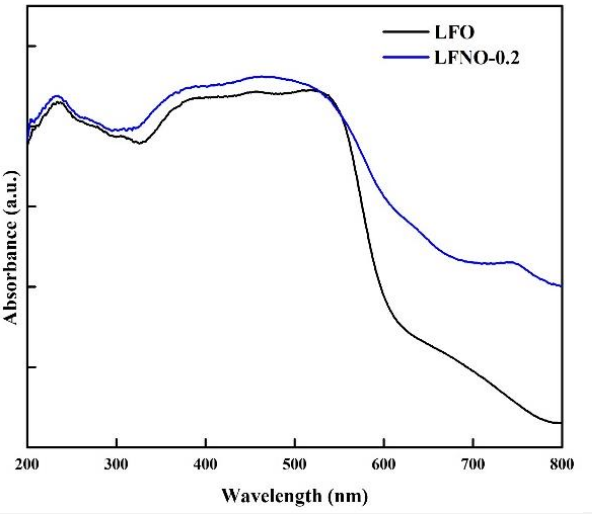


**Fig. 3.** UV-Visible absorption spectra of LFO and LFNO-0.2 samples.

The LFO and LFNO-0.2 photocatalysts deliver the highest degradation efficiency of ~84.08, and ~89.44%, respectively. The better degradation performance of LFNO-0.2 is ascribed to the porous structure which provides large active sites for dye-adsorption on the surface of catalyst. The Langmuir-Hinshelwood model was applied to understand the kinetics of photocatalytic degradation reaction Eq. 2,

$$-\ln C_t/C_0 = k_{obs} \cdot t \quad (2)$$

where, $C_0$ and $C_t$ represent the initial and final dye concentration, respectively, t represents the degradation time, and $k_{obs}$ represent the pseudo-1$^{st}$-order rate constant. The reaction kinetics was approximated from ($Ct/C_0$) and –ln ($C_t/C_0$) vs time plots, respectively. Fig. 4(d, e) shows the effect of LFO catalysts on the kinetics of photocatalytic RhB dye degradation. The rate constant of 0.01034 and 0.01304 $min^{-1}$ was estimated for LFO and LFNO-0.2 catalyst. Furthermore, the coefficient of correlation ($R^2$) for LFO and LFNO-0.2 was estimated ~0.982 and ~0.989, respectively, which confirms that LFNO-0.2 accomplished better for the photocatalytic degradation of RhB dye.

Furthermore, cyclic stability was evaluated for the LFNO-0.2 sample for real-time applicability. During cyclic stability measurements, the powder was washed and collected by centrifugation and dried in the open atmosphere after each experiment. The same powder was again used for another cycle of dye degradation. Fig. 5(a-c) shows UV-Visible absorption spectra for three consecutive cycles and observed excellent cyclic stability (Fig. 5(d)) for the LFNO-0.2 sample. Moreover, isopropyl alcohol, methyl alcohol, and ammonium oxalate scavengers were used to check the impact of hydroxyl ($\cdot OH^-$) and superoxide radicals ($\cdot O_2^-$) along with photo-generated holes ($h^+$), respectively, on the degradation performance of RhB dye.

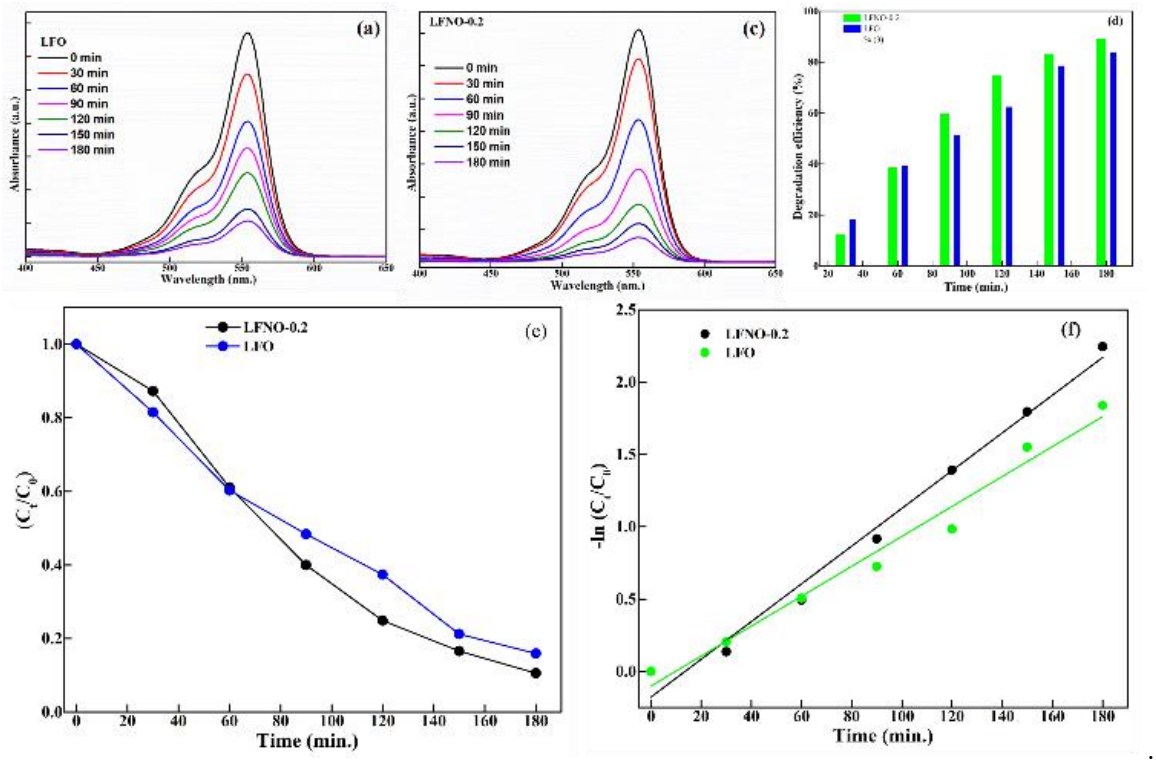


**Fig. 4.** Time-dependent UV-Visible spectra of 30 mg (a) LFO, and (b) LFNO-0.2 for 30 ppm RhB dye, (c) histogram of degradation, (d) Kinetic plot, and (e) Langmuir Hinshelwood model using 30 mg catalyst.

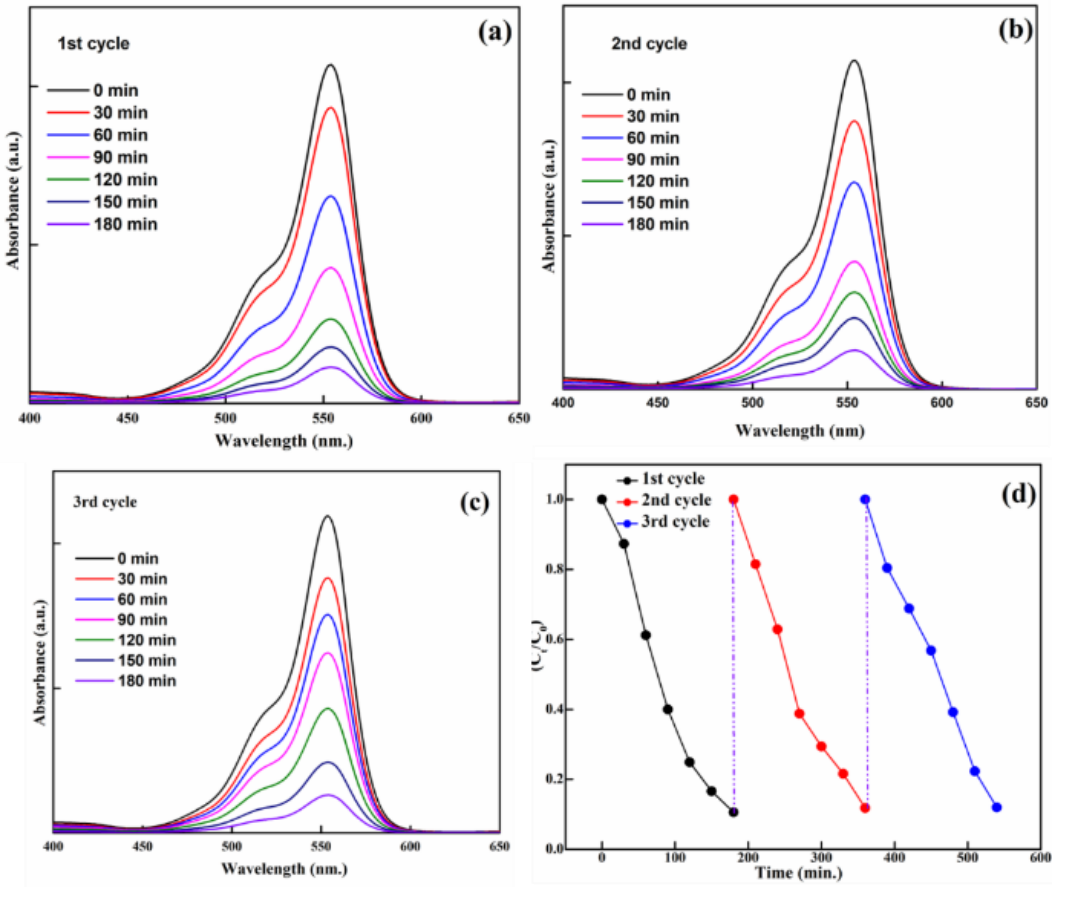


**Fig. 5.** UV-Visible spectra for (a) First, (b) second, (c) Third cycle, and (d) cyclic stability performance of RhB dye degradation using LFNO-0.2 catalyst.

 

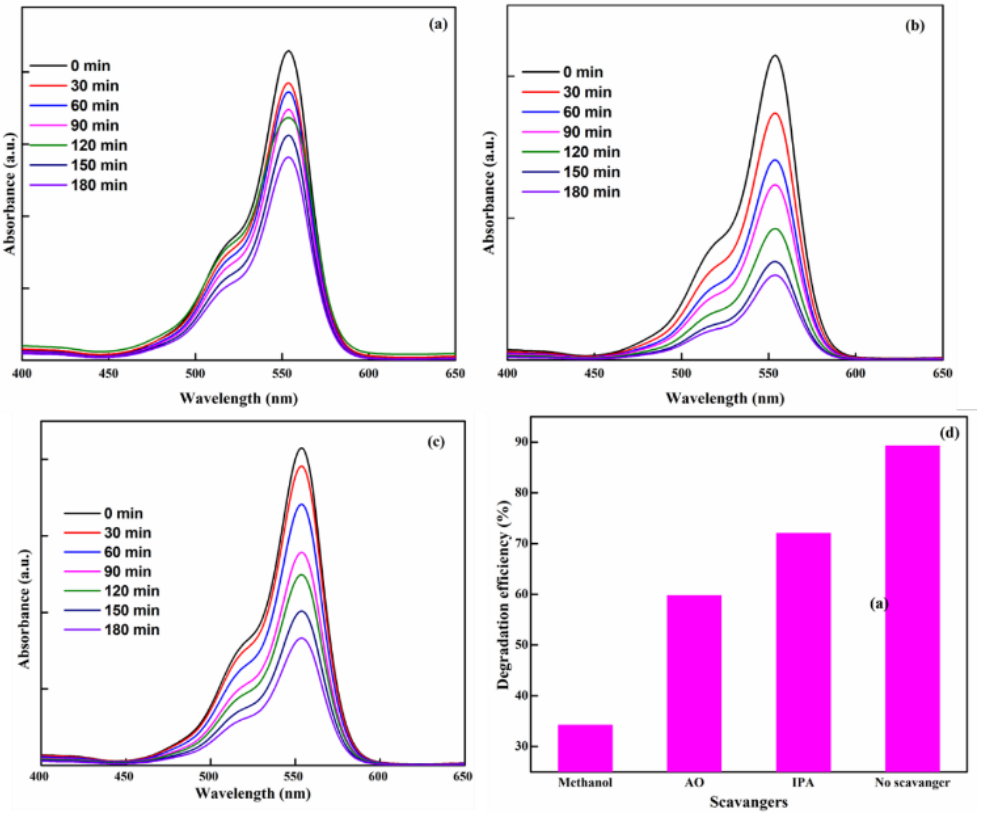


**Fig. 6.** UV-Visible absorption plot for different scavengers (a) methanol, (b) IPA, and (c) ammonium oxalate, and (d) effect of scavenger represented in terms of histogram using LFNO-0.2 catalyst.

The photo-degradation behavior of RhB dye in the presence of various scavengers (Fig. 6(a-c)) indicates the significant quenching in the degradation of RhB due to methyl alcohol ($\cdot O_2^-$ radicals, Fig. 6(d)). The adequate reduction in the degradation efficiency in the presence of AO demonstrates the active role of photogenerated holes. Likewise, a moderate decrease in degradation efficiency in IPA indicates the partial involvement of hydroxyl radicals. The above observations confirmed that $O_2^-$ and photogenerated $h^+$ from LFNO-0.2 samples significantly influenced the photodegradation of organic dye.

To check whether the given material is stable under the photocatalytic dye degradation experiment XRD of the sample before and after the photocatalytic experiment was performed. For this, the material treated under Xenon lamp for photocatalytic dye degradation was collected by centrifugation, and after drying, the XRD of the sample was taken. Fig. 7 shows the XRD spectra of the pristine LFNO-0.2 microsphere consisting of nanoparticles and centrifugally extracted LFNO-0.2 after the photocatalytic reaction. The XRD spectra of pristine and centrifugally extracted (i.e., photo-reacted) LFNO-0.2 samples are akin to each other and display the XRD peaks at 2θ of 22.9, 27.9, 32.3, 39.5, 46.6, 52.1, 57.3, 67.3, and 76.8º corresponding to the (101), (111), (121), (220), (202), (141), (240), (242), and (204) planes, respectively, of orthorhombic crystal. All these peaks are analogous to the peaks corresponding to LFNO, as reported in the literature.

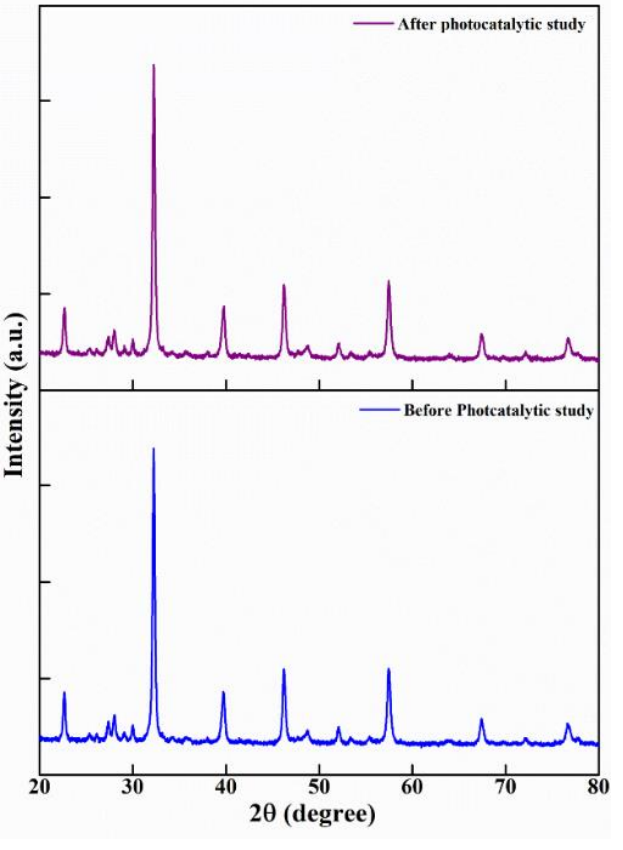


**Fig. 7.** XRD pattern of LFNO-0.2 before and after the three consecutive cycles of photocatalytic RhB dye degradation.

## 4. CONCLUSIONS

LFO and LFNO-0.2 samples are successfully synthesized by hydrothermal method for utilization of photocatalytic degradation of RhB organic dye. XRD analysis confirms the successful doping of $Ni^{2+}$ at the $Fe^{3+}$ site in the LFO lattice. The FESEM analysis indicates the formation of microsphere-like morphology, which consists of nanoparticles. The absorption of the whole solar spectrum is responsible for getting superior activity for RhB dye degradation. The LFO and LFNO-0.2 deliver the photocatalytic degradation activity of 84.08 and 89.44% with rate constant and correlation coefficient of 0.01034, and 0.01304 $min^{-1,}$ and 0.982 and 0.989, respectively. The scavenger active radical trapping experiment confirms the active involvement of $O_2^-$ and $h^+$ in the degradation of RhB. The LFNO-0.2 provides good cyclic stability up to three consecutive cycles of degradation and shows good structural stability post to the degradation experiment. Therefore, the Ni-doped LFO can be considered as the cost-effective and efficient catalyst for the degradation of organic dye.

## CONFLICT OF INTEREST

The authors declare that there is no conflict of interests.

## ACKNOWLEDGEMENTS

The authors would like to thank the Science and Engineering Research Board (SERB), DST-Ministry of Science and Technology, Board of Research in Nuclear Sciences (BRNS), and National Technical Textile Mission (NTTM) Ministry of Textile for their financial support for this research under grant no. CRG/2022/000160, DST/WOS-A/PM-118/2021, 58/14/08/2023/BRNS/11687 and 2/1/2023/NTTM, respectively. SRM acknowledge the INSPIRE research fellowship IF/180222 from DST India.

## REFERENCES

[1] Patil M. S., Kitchamsetti N., Mulani S. R., Rondiya S. R., Deshpande N. G., Patil R. A., Cross R. W., Dzade N. Y., Sharma K. K., Patil P. S., Ma Y.-R., Cho H. K., Devan R. S., **2021**, Photocatalytic behavior of $Ba(Sb/Ta)_2O_6$ perovskite for reduction of organic pollutants: Experimental and DFT correlation, *Journal of the Taiwan Institute of Chemical Engineers*, 122, pp. 201-209.

[2] Kitchamsetti N., Didwal P. N., Mulani S. R., Patil M. S., Devan R. S., **2021**, Photocatalytic activity of $MnTiO_3$ perovskite nanodiscs for the removal of organic pollutants, *Heliyon*, 7, pp. e07297.

[3] Akerdi A. G., Bahrami S. H., **2019**, Application of heterogeneous nano-semiconductors for photocatalytic advanced oxidation of organic compounds: A review, *Journal of Environmental Chemical Engineering*, 7, pp. 103283.

[4] Crini G., Lichtfouse E., **2019**, Advantages and disadvantages of techniques used for wastewater treatment, *Environmental chemistry letters*, 17, pp. 145-155.

[5] Bimli S., Mulani S. R., Choudhary E., Manjunath V., Shinde P., Jadkar S. R., Devan R. S., **2024**, Perovskite $BaSnO_3$ nanoparticles for solar-driven bi-functional photocatalytic activity: PEC water splitting and Wastewater treatment, *International Journal of Hydrogen Energy*, 51, pp. 1497-1507.

[6] Chen D., Cheng Y., Zhou N., Chen P., Wang Y., Li K., Huo S., Cheng P., Peng P., Zhang R., **2020**, Photocatalytic degradation of organic pollutants using $TiO_2$-based photocatalysts: A review, *Journal of Cleaner Production*, 268, pp. 121725.

[7] Di Paola A., García-López E., Marcì G., Palmisano L., **2012**, A survey of photocatalytic materials for environmental remediation, *Journal of hazardous materials*, 211, pp. 3-29.

[8] Dutta V., Sharma S., Raizada P., Thakur V. K., Khan A. A. P., Saini V., Asiri A. M., Singh P., **2021**, An overview on $WO_3$ based photocatalyst for environmental remediation, *Journal of Environmental Chemical Engineering*, 9, pp. 105018.

[9] Sun C., Yang J., Xu M., Cui Y., Ren W., Zhang J., Zhao H., Liang B., **2022**, Recent intensification strategies of $SnO_2$-based photocatalysts: A review, *Chemical Engineering Journal*, 427, pp. 131564.

[10] Fauzi A., Jalil A., Hassan N., Aziz F., Azami M., Hussain I., Saravanan R., Vo D.-V., **2022**, A critical review on relationship of $CeO_2$-based photocatalyst towards mechanistic degradation of organic pollutant, *Chemosphere*, 286, pp. 131651.

[11] Kitchamsetti N., Ramteke M. S., Rondiya S. R., Mulani S. R., Patil M. S., Cross R. W., Dzade N. Y., Devan R. S., **2021**, DFT and experimental investigations on the photocatalytic activities of NiO nanobelts for removal of organic pollutants, *Journal of Alloys and Compounds*, 855, pp. 157337.

[12] Aldeen E. S., Jalil A., Mim R., Alhebshi A., Hassan N., Saravanan e., **2022**, Altered zirconium dioxide based photocatalyst for enhancement of organic pollutants degradation: A review, *Chemosphere*, 304, pp. 135349.

[13]Wang W., Tadé M. O., Shao Z., **2015**, Research progress of perovskite materials in photocatalysis-and photovoltaics-related energy conversion and

 

environmental treatment, *Chemical Society Reviews*, 44, pp. 5371-5408.

[14] Iervolino G., Vaiano V., Sannino D., Rizzo L., Palma V., **2017**, Enhanced photocatalytic hydrogen production from glucose aqueous matrices on Ru-doped $LaFeO_3$, *Applied Catalysis B: Environmental*, 207, pp. 182-194.

[15] Thirumalairajan S., Girija K., Mastelaro V. R., Ponpandian N., **2015**, Investigation on magnetic and electric properties of morphologically different perovskite $LaFeO_3$ nanostructures, *Journal of Materials Science: Materials in Electronics*, 26, pp. 8652-8662.

[16] Phan T. T. N., Nikoloski A. N., Bahri P. A., Li D., **2018**, Optimizing photocatalytic performance of hydrothermally synthesized $LaFeO_3$ by tuning material properties and operating conditions, *Journal of Environmental Chemical Engineering*, 6, pp. 1209-1218.

[17] Kumar R., Choudhary R., Khan M. W., Srivastava J., Bao C., Tsai H., Chiou J., Asokan K., Pong W., **2005**, Structural, electrical transport and x-ray absorption spectroscopy studies of $LaFe_{1-x}Ni_xO_3$ ($x \leqslant 0.6$), *Journal of Applied Physics*, 97, pp. 093526.

[18] Pecchi G., Reyes P., Zamora R., Cadus L., Fierro J., **2008**, Surface properties and performance for VOCs combustion of $LaFe_{1-y}Ni_yO_3$ perovskite oxides, *Journal of Solid State Chemistry*, 181, pp. 905-912.

[19] Mulani S. R., Bimli S., Choudhary E., Bunkar R., Kshirsagar U. A., Devan R. S.,**2023**, Cationic and anionic cross-assisted synergistic photocatalytic removal of binary organic dye mixture using Ni-doped perovskite oxide, *Chemosphere*, 340, pp. 139890.

[20] Mulani S. R., Bimli S., Choudhary E., Jadhav H., Jangir R., Shaikh P. A., Devan R. S., **2024**, Infrared active narrow bandgap Ni doped $LaFeO_3$ nanoparticles for desalination and decontamination of water leveraging interfacial solar steam generation, *Desalination*, 574, pp. 117298.

[21] Hao P., Lin Z., Song P., Yang Z., Wang Q., **2020**, Hydrothermal preparation and acetone-sensing properties of Ni-doped porous $LaFeO_3$ microspheres, Journal of Materials Science: Materials in Electronics, 31, pp. 6679-6689.

[22] Mulani S. R., Bimli S., Patil M. S., Kshirsagar U. A., Devan R. S., 2023, Porous $LaFeO_3$ walnuts for efficient visible light driven photocatalytic detoxification of harmful organic pollutants, Materials Chemistry and Physics, 305, pp. 127952.

 